geographies

MDPI

Article

Photogrammetry from UAV and Low-Cost Lidar for Sinkhole Hazard Mitigation in Urban Areas: Applications and Evaluations

Francesco Gentili [1,*] and Sergio Madonna [2]

[1] Department of Ecological and Biological Sciences, Tuscia University, Via San Camillo De Lellis snc, 01100 Viterbo, Italy
[2] Department of Agriculture and Forest Sciences, Tuscia University, Via San Camillo De Lellis snc, 01100 Viterbo, Italy; sermad@unitus.it
* Correspondence: francesco.gentili@unitus.it

Abstract: The Italian national territory is characterised by the widespread presence of cavities dating back to different periods, especially in urban areas. The lack of knowledge of the position of the entrances, planimetric developments and state of preservation contributes to accentuating the unknowns related to sinkhole risk, which are directly related to potential cavity collapses with the opening of surface chasms. To deepen knowledge with a view to risk mitigation, a method has been developed to employ surveys obtained from Unmanned Aerial Vehicles (UAVs) to locate entrances even in hard-to-access urban areas. These surveys, properly supported with GNSS stations, were then integrated with cavity surveys obtained from low-cost lidar mounted on iPhones. Comparisons were made with traditional surveying techniques to better understand the reliability of the surveys made with low-cost lidar. The 3D models obtained, combined with geomechanical surveys of the rock masses hosting the cavities, allowed the application of simplified and empirical methods for an initial stability assessment. This method was tested on a portion of the municipality of Grotte di Castro (Province of Viterbo—Italy).

Keywords: sinkhole; photogrammetry; UAV; lidar; iPhone; geomechanical survey

Citation: Gentili, F.; Madonna, S. Photogrammetry from UAV and Low-Cost Lidar for Sinkhole Hazard Mitigation in Urban Areas: Applications and Evaluations. *Geographies* **2024**, *4*, 343–362. https://doi.org/10.3390/geographies4020020

Academic Editor: Xu Chen

Received: 29 April 2024
Revised: 14 May 2024
Accepted: 27 May 2024
Published: 30 May 2024

1. Introduction

Italy is characterised by diversified geological hazards mainly related to landslides, floods, volcanic activity and widespread seismicity. However, there are also less known and often neglected forms of geological hazard, such as sinkholes. The spread of built-up areas and the presence of infrastructures transform this hazard into a risk. The term sinkhole indicates a subcircular cavity that opens suddenly on the surface, and is used as a synonym for collapse [1,2]. Two main genetic groups of natural sinkholes can be found: solution sinkholes resulting from internal erosion processes caused by subsurface karstification of carbonates or evaporites, and solution-induced subsidence processes that may affect cover deposits over karst and non-karst bedrock [3,4]. The natural origin sinkholes particularly affect extra-urban areas, while most of the sinkholes that develop in urban areas are of anthropogenic origin and connected to the collapse of underground cavities dug by man or leaks of networks and subsystems [2,5].

The Latium region, like several others in Italy [6–10], is characterised by the presence of small towns like Grotte di Castro but also large and densely populated cities like Rome, that have a subsoil rich in cavities, especially of anthropogenic origin. These underground structures' functions vary due to their types and origins: hydraulic works, cellars, tombs, necropolis, catacombs, worship places, shelters, etc. In the Tuscia area, some centres, such as Viterbo (Provincial capital), Bolsena and Montefiascone, have already been the subject of a preliminary census [11,12], but the majority lack any data. To mitigate this risk, of primary importance is the development of methodologies and guidelines that will lead to

the identification and census of cavities, and then assessing their state of stability to sample whether sinkholes may originate.

The use of UAVs is highly versatile for land mapping issues for geoscience purposes [13,14] and, in recent times, also in the study and monitoring of natural sinkholes [15], suggesting that they can also be applied to the search for and census of artificial cavities whose location is unknown. Technological progress in recent years has led to the miniaturisation of some lidar instruments and the possibility of installing them on smartphones and other wearable devices. Since the 12 Pro series, iPhones have been fitted with lidar sensors capable of detecting the surrounding space and providing 3D models and point clouds of the spaces and objects detected. The potential of these instruments has been evaluated in surveying small areas, finding good margins of applicability [16] even by mounting these systems on low-cost UAVs [17]. Other studies [18,19] have evaluated these surveying methods in indoor and outdoor environments, suggesting possible ways of application and surveying, finding local accuracies on the millimetre scale. The positive evaluations also found in surveying underground structures [20] led to surveying applications in artificial cavities in tuffaceous rock masses, typical of settlements in central Italy. Also considering other previous experiences in which photogrammetry and orthophotos from UAVs have been used in combination with lidar surveys [21], we connect photogrammetric surveys from UAVs and lidar surveys from iPhones for the construction of 3D models for the study of cavities, interactions with the surface and initial assessments of stability. Comparisons were made with traditional survey methods to verify reliability on this scale. Geomechanical surveys were carried out according to procedures defined in the literature [22–24] to apply empirical methods for [25–27], some of which have already been used in recent and related studies [28]. This paper assessed the possibility of using these lidar surveys in combination with photogrammetric surveys (at different levels of accuracy) for approaches to the cavity census and assessing the stability of the cavities.

2. Study Area

The municipality of Grotte di Castro is known for having a significantly large number of underground cavities. Since the Etruscan and Roman Ages, these cavities have been excavated and, in different periods, often remodelled, enlarged and transformed for other uses, especially from the medieval era to the present. Specific archaeological and geophysical research has only been carried out on a limited number of them [29]. According to reports such as the Hydrogeological Structure Plan of "Autorità di Bacino Distrettuale dell'Appennino Centrale" and the Sinkhole susceptibility map of the Lazio Region [30], the entire area is potentially at risk due to these cavities. However, currently, there is no census of these underground cavities. This makes this site the ideal place to experience new methods that can lead to a rapid census and, at the same time, provide preliminary indications of their stability.

2.1. Geological Context

The study area is located in the Latera Volcanic Complex of the Quaternary Vulsini Volcanic District (VVD), which forms the northern part of the so-called "Alkali-potassic Roman Magmatic Province" [31], a belt of young volcanoes aligned along the western coast of Italy (Figure 1). The VVD consists of partially superimposed multicentre volcanic complexes (over 100) and includes calderas (Montefiascone, Latera, Vepe) developed around the polygenic volcano-tectonic depression of the Bolsena Lake. Eruptions cover over 2200 km^2 and embody more than 40 km^3 of ignimbrites, pyroclastic fall deposits, minor pyroclastic surges, lavas and cinder cones [32,33]. The composition ranges from Potassic trachybasalt to trachyte, ultrapotassic leucitite and leucite tephrite to phonolite [34]. The VVD developed along a graben (Paglia-Tevere) and horst (M. Razzano) system and the pre-volcanic rocks include Liguride, Tuscan and Umbria sequences. The VVD (Figure 1) consists of five major volcanic complexes. The first four; Paleo-Vulsini (about 1.3–0.49 M.a), Bolsena-Orvieto (about 0.49–0.3 Ma), Montefiascone (about 0.3 to 0.2 Ma) and Latera

(about 0.28–0.14 Ma); were identified by most authors [34–39], but more recently Palladino et al. 2010 [40] and Acocella et al. 2012 [41] introduced the Southern Vulsini complex (0.4–0.13 Ma). For the Paleo-Vulsini, activity in the NE sector of the Bolsena [42,43] shifts the onset of volcanism to about 1.7 Ma.

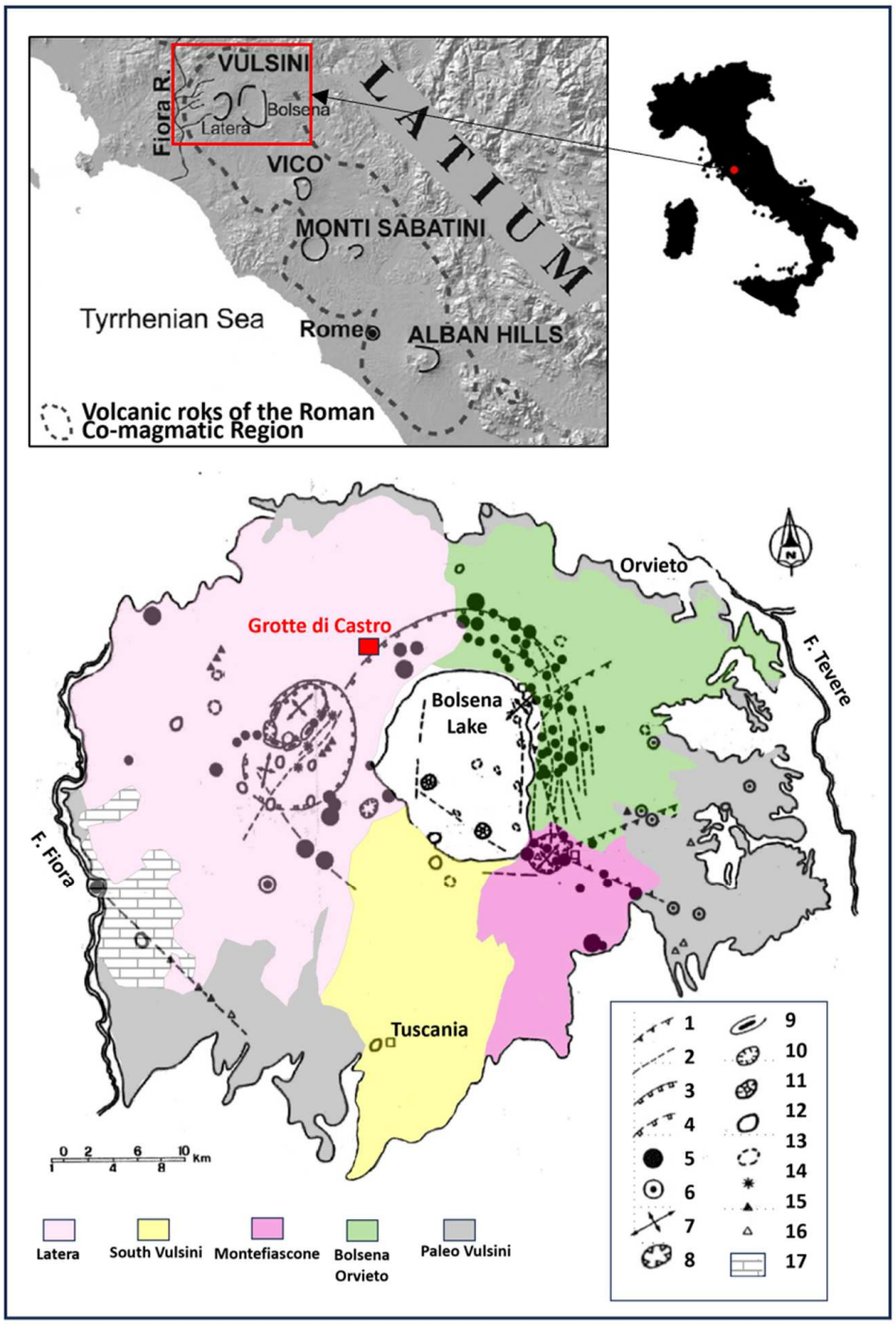

Figure 1. Structural map of the Vulsini Volcanic District (VVD): (**1**) Deep faults; (**2**) Faults; (**3**) Caldera rim; (**4**) Buried caldera rim; (**5**) Cinder cones; (**6**) Buried cinder cones (**7**) Central explosive eruptions; (**8**) Travertine; (**9**) Maar; (**10**) Dome-like structures; (**11**) Explosion craters; (**12**) Surtseyan activity; (**13**) Eruptive centres; (**14**) Buried eruptive centres; (**15**) Sulphurous activity: (**16**) Thermomineral springs; (**17**) Main mineral springs (after Nappi Renzulli and Santi, 1987 and Peccerillo, 2017; modified and partially redrawn).

2.2. Geomorphological and Stratigraphic Setting

Grotte di Castro (Figure 1) is located on the northern rim of the Bolsena Caldera on a plateau produced by the pyroclastic flow deposits of the Latera Volcanic Complex and subsequently shaped by fluvial processes, especially during the Last Glacial Maximum (LGM). The small town lies on a cliff, limited on three sides by steep slopes with high and very high landslide hazards. Moreover, as mentioned above, the whole area of the old town is considered an attention zone (AA) for the presence of artificial cavities subject to collapse (Figure 2). Flood hazard is limited to the lower part of the valley at the confluence of the "Fosso dei Piselli" with the ditch (without a name) that borders the historic centre to the north, both confluent in the "Il Fiume" river and then in the Bolsena Lake.

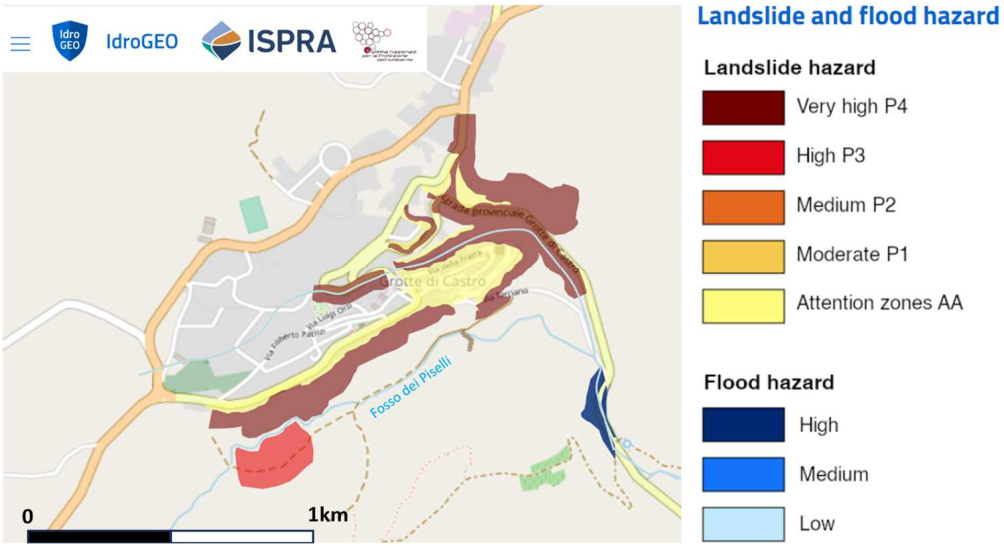

Figure 2. Landslide and flood hazard map of Grotte di Castro from IdroGEO, The Italian web platform on landslides and floods, hazards and risk (ISPRA 2020 Pericolosità e indicatori di rischio per frane e alluvioni) [44]. Attention zones (AAs) indicate the presence of cavity systems.

For the study area, there is no more up-to-date cartography than the obsolete sheet 129 of the Italian Geological Map in scale 1:100,000 [45], and, to the best of our knowledge, detailed geological studies analysing the complex organisation of volcanic units in the area do not exist. The geological scheme we propose (Figure 3) has been realised following a lithological criterion and includes huge subdivisions that combine several volcanic units. However, the presence of two outcrops (highlighted in the geological map) in which the volcanic succession has been investigated in detail [46] allows a possible correlation with the geologic formations described in the most recent literature [41]. The upper Latera tuffaceous complex (4—in Figure 3) includes the following volcanic units: the Grotte di Castro Formation (at the base) followed by the Onano/Poggio Pinzo Formation and (at the top) the Pitigliano Formation. The lower Latera tuffaceous complex (5—in Figure 3) includes the Sorano Formation (at the top), the Sovana Formation and probably the Farnese and the Canino Formations (at its base). However, the underground cavities forming the object of this study develop only within the Grotte di Castro Formation and the underlying Sorano Formation. Locally, the lower part of the Grotte di Castro Formation (GRC) comprises a few metres of thick planar and cross-bedded ash and vesiculated tuffs with accretionary lapilli, followed by an ash flow deposit: middle consolidated yellow glassy ash with scattered yellow pumices, grey pumices and lithics. The Sorano Formation represents the upper part of the lower tufa complex (5—in Figure 3). Locally, at the top, at the passage with the Grotte di Castro Formation, highly consolidated ash flow deposits occur with a pink–yellow ashy matrix and yellowish or white scattered, light grey pumices and rare lithic. Under them, very consolidated ash flow deposits are present, with a light yellow ashy matrix, subparallel lineation, white pumices and columnar jointing.

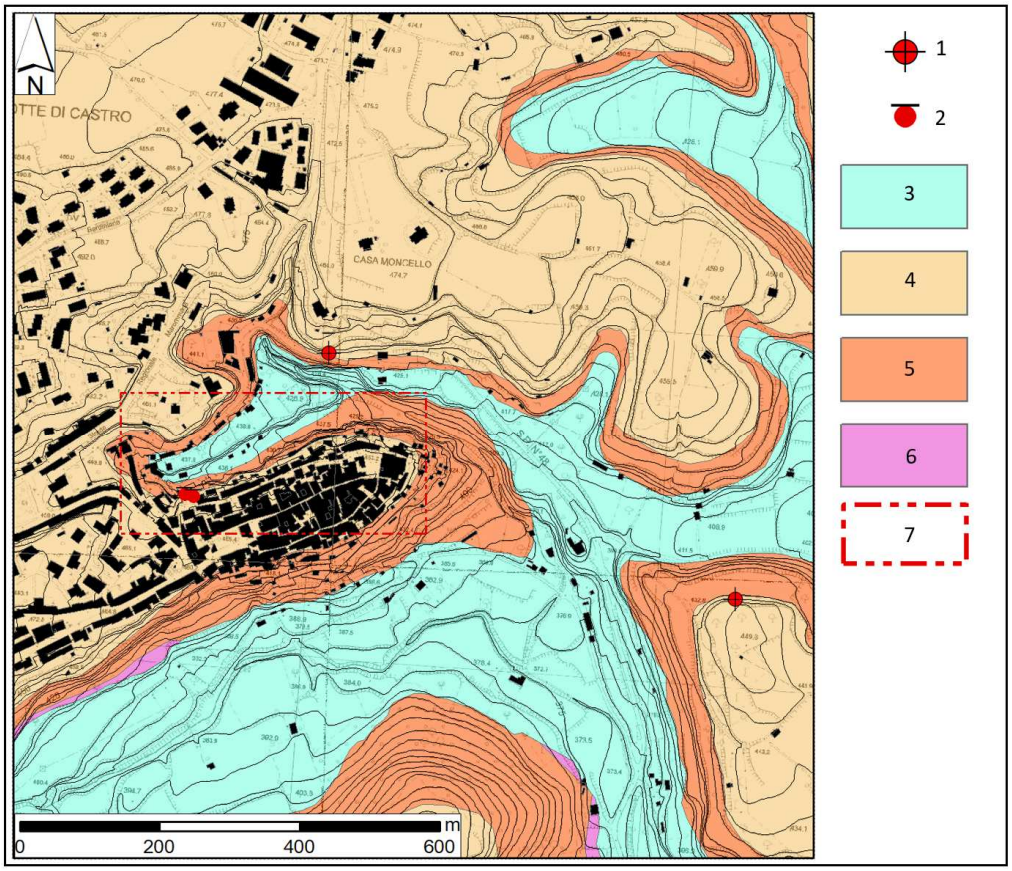

Figure 3. Geological schematic map of Grotte di Castro urban area: (**1**) Key outcrop; (**2**) Investigated cavities; (**3**) Alluvial, eluvium colluvium and slope deposits; (**4**) Upper Latera tufa complex; (**5**) Lower Latera tufa complex; (**6**) Lava flow unit; (**7**) UAV surveyed area.

3. Materials and Methods

UAV photogrammetric flights made it possible to obtain 3D models of the northern cliffs of Grotte di Castro and to facilitate the localisation of cavity entrances. Only two cavities could be surveyed from the inside, using the iPhone lidar manually and traditional topographic methods. The 3D models from the UAV and iPhone lidar were aligned and merged into a single model using ground markers (Figure 4B–D). The cavities were also geomechanically surveyed to assess their geotechnical and structural characteristics.

3.1. Photogrammetric Surveys

Days with good weather conditions and low wind speeds (less than 7 knots) were considered to execute the UAV flights. To limit urban clutter problems, such as vehicular traffic, the flight was performed on public holidays and in the early morning hours (7–9 am). Photogrammetric surveys were carried out using the DJI Mavic Pro UAV equipped with onboard camera. The vehicle's small size is well suited to urban contexts, simplifying piloting conditions and facilitating surveying patterns. To compensate for the limited characteristics of the onboard camera, the surveying pattern was planned with the camera in a nadiral position (−90°) with an estimated photographic overlap of 80%, at a speed of approximately 3 m/s and at an altitude of 40 m from the take-off point, located on the summit portion of the cliff to avoid reductions in the photographic overlap. The images were also acquired with manual flights, camera in a frontal position (0°–25°) and at a low altitude (25–30 m), frontally framing the built-up area and the neighbouring slopes at an estimated distance of approximately 30–35 m. The low flight speed combined with the optimal lighting conditions related to the time of day helped to limit possible distortion and blurring effects in the photographs. In total, 589 images were taken and stored on a

high-speed memory card. To obtain a high-precision survey, nine markers were placed on the ground (Figure 4A), the centre of which was measured with the Leica GNSS station consisting of GS08 plus rover, CS10 controller and 2 m rod, connected to Leica's Smartenet network. The geographical coordinates obtained (ETRF 2000) were transformed into Monte Mario Italy I (EPSG 3003) projected coordinates using the IGM GK2 grid No. 333, containing the geoid model Italgeo 2005. The photogrammetric process involved the use of AgisoftMetashape Professional software (version 1.6.3 build 10732). First, the quality of the images was assessed using the Metashape tool Estimate Image Quality. The photos obtained had quality values between 0.69 and 1.07. Only images with quality values greater than 0.75 were considered for the survey, which resulted in only four images being eliminated beforehand. Using 585 images, the sparse cloud was created, and the reference system (EPSG 3003) was given, assigning each marker found in the photos the coordinates processed from the GNSS measurements (Figure 4A). The markers were divided into Ground Control Points (GCP) and Control Points (CP) to estimate the errors in the survey. The sparse cloud was first subjected to the alignment optimisation and Gradual Selection process, removing points from the sparse cloud to improve reconstruction uncertainty, projection accuracy and reprojection error. This sequential processing further reduced the error associated with the survey. Following the workflow, the high quality dense cloud was generated, then edited by removing low confidence points and classifying it. From the point cloud, we obtained the texturised 3D model and DEM, with the latter used for the realisation of the orthomosaic. To evaluate a faster and more flexible use of drone photogrammetry, a 3D model, with average quality, was created using data from the Mavic Pro's onboard GPS in wgs84 geographic coordinates without using GNSS station data. This model was used to identify the cavity entrances quickly. A field survey was then carried out to locate the cavity entrances for comparison.

3.2. Lidar Surveys and Traditional Surveys

It was possible to access two cavities, which were detected by lidar mounted on an iPhone 15 Pro Max using the Scaniverse application. The iPhone 15 Pro Max uses the SPAD Sony IMX591 ToF-type lidar sensor with an estimated resolution of 0.01 mega-pixels and a pixel pitch of 10.1 microns. In both cavities, specific markers were placed on the walls (Figure 4D) as it was planned to survey them in portions. The markers, always at least four in common for contiguous portions, were later used to assemble the portions to limit alignment-related errors. For the alignment, the open-source software Cloud Compare version 2.1 [47] was used with the Alings Two Clouds tool, which requires at least 4 points in common between the cloud (or model) to be aligned and the cloud (or model) used as a reference. The alignment process initially involved joining the lidar survey exterior to the georeferenced photogrammetric survey with GNSS station using specific markers (Figure 4B,C). Using the Merge Multiple Clouds tool, both the aligned models and the aligned point clouds were merged into a single product, exported in the native coordinate and elevation system of the photogrammetric survey (EPSG 3003 with orthometric elevations), the details of which are shown in Figure 5B,C. Using Cloud Compare's Compass tool, it was possible to identify the main fractures of the rock mass on the georeferenced merged 3D model. This facilitated the application of stability assessment methods, in particular the Graphical Stability Method. To verify the reliability of the lidar surveys of the iPhone 15 Pro Max, the same cavities were in turn surveyed using traditional techniques, which involved the use of metric webbing and the Leica Disto X3-1, linked to the Disto Plan application, which allowed the cavity plans to be obtained directly in .dxf files.

Figure 4. Examples of markers used for georeferencing the photogrammetric survey with a GNSS station in Agisoft Metashape (**A**), aligning lidar surveys (**C**) to the photogrammetric survey (**B**) and facilitating the alignment of the lidar survey portions of cavities (**D**).

3.3. Geomechanical Survey

Geomechanical and fracture surveys were conducted in both cavities to classify the rock mass according to Barton's Q method [48–50]:

$$Q = \left(\frac{RQD}{Jn}\right) \times \left(\frac{Jr}{Ja}\right) \times \left(\frac{Jw}{SRF}\right) \quad (1)$$

where:

RQD (Rock Quality Designation) considers the rock mass's subdivision.

Jn (Joint Set Number) depends on the number of joint families in the rock mass.

Jr (Joint Roughness Number) depends on the roughness of the most unfavourable family.

Ja (Joint Alteration Number) depends on the degree of fracture alteration, thickness and nature of the fill, and is also determined by the most unfavourable family.

Jw (Joint Water Number) depends on hydrogeological conditions.

SRF (Stress Reduction Factor) is a function of the stress state in massive rocks or tectonic disturbance.

The Geostone rock sclerometer, Standard ISMRs, a profilometer, a metric tape and a geologist's compass were used to determine the *Q* value.

3.4. Basic Methods for Stability Assessment

For illustrative purposes to evaluate the use of the 3D models obtained, data from UAV, lidar and geomechanical surveys were used to estimate these cavities' stability. To do this, three empirical methodologies known from the literature were examined. The first to have been used was the Critical Scaled Crow Span [26,51], according to which vault instability is probable if the scaled crow span *Cs* is greater than the critical span Sc. *Cs* can be calculated using the following equation:

$$Cs = \sqrt{(\gamma}/T\left(1 + \frac{S}{L}\right)(1 - 0.4cos\theta)) \quad (2)$$

where:

S = clear span of the vault in metres

L = length of the vault in metres

T = thickness of the vault in metres

γ = specific gravity of the rock mass (1.8 t/m^3)

θ = deep direction of the stratification

The critical light *Sc*, on the other hand, can be calculated using the following equation:

$$Sc = 3.3Q^{0.43}\left(senh^{0.0016}(Q)\right) \quad (3)$$

where Q is determined by classification of the Barton rock mass.

Also examined is The Graphical Stability Method [27] which evaluates the stability of a cavity based on the stability number N, which is given by the following equation:

$$N = Q\prime \times A \times B \times C \quad (4)$$

where:

$Q\prime$ = Barton classification with *SFR* = 1 and *Jw* = 1

A = rock stress factor, which is calculated graphically based on the ratio σc/σl. σc is the unconfined compressive strength of the intact rock and was estimated using sclerometric tests and ISMR Standards. σl is induced compressive stress, estimated from published stress distribution [52–54].

B = joint orientation adjustment factor, which depends on the difference between the orientation of the critical joint and each face of the stope, which can be found graphically.

C = gravity adjustment factor, which can be calculated graphically and assesses mobilisations by falls and sliding.

The stability number N thus determined is compared with the hydraulic radius S of the cavity, which is given by the ratio of surface area to perimeter. From the stability graph it is possible to assess the degree of stability of the cavity.

The last methodology used was the one proposed by [25], which evaluates the propensity for slope collapse in a seismic event with M > 5. The methodology is based on the Q parameter of the Barton classification modified according to the following equation:

$$Q'' = \left(\frac{(115-3)Jv}{Jn}\right)\left(\frac{Jr}{Ja}\right)\left(\frac{1}{AF}\right) \quad (5)$$

Jv represents the number of joints per $m^{3,}$ and AF considers the discontinuity's opening. In the case of tunnels in the zone of entry, Jn is to be doubled, and in the zone of intersection of two tunnels, Jn is to be tripled. The propensity to collapse is qualitatively defined by the value of Q, according to Table 1.

Table 1. Susceptibility to collapse based on the value of Q.

Q″	Susceptibility to Collapse for Seismic Event of Magnitude > 5
<0.1	Very high
0.1–1	High
1–9.99	Medium
>10	Low

4. Results

4.1. Photogrammetry

UAV flights returned surveys with very different errors depending on the type of GPS used for scaling, as Table 2 shows.

Table 2. Errors associated with the surveys and lead times (excluding the photogrammetric process).

GPS	Error (m)	Lead Time (Minutes)
GNSS Station	0.037 (on GCP) 0.043 (on CP)	68
Mavic Pro GPS	1.7	21

Using the same photographic dataset, the same number of cavity entrances along the slopes of the north cliff were counted in both surveys. A total of 76 entrances were counted on 3D models and photos (Figure 6). The survey on foot along the cliff made it possible to survey 58 entrances, the coordinates of which were recorded using a standard GPS mounted on smartphones, with an error similar to that associated with the on-board GPS of the Mavic Pro. It took 2 h and 25 min to carry out the survey. The results of the comparison between the two census methods are shown in Table 3.

Table 3. Results obtained from the two census methods (the time taken with the UAV method also includes the time taken to create the 3D model and search for cavities on it).

Method	Number of Entrances	Lead Time (Minutes)
UAV Model	76	64
Reconnaissance	58	145

4.2. Lidar Surveys and Traditional Surveys

The two cavities surveyed comprised one entrance, two rooms and one tunnel (cavity n1) and one entrance, three rooms and two tunnels (cavity n2), respectively. The point clouds and 3D models textured from the iPhone 15 Pro Max lidar of the cavities were aligned using the Cloud Compare command. The procedure already described first saw the 3D models of the exteriors aligned with the high-precision model obtained from the UAV survey, which was taken as a reference due to its associated degree of accuracy. For each alignment of the cavity portions, the software calculated an RMS and a scaling factor.

For each alignment, averages were taken to calculate an error associated with the cavity, as shown in Table 4.

Table 4. Error alignment and scaling factors.

Cavity	RMS (m)	Scale Factor
1	0.035	0.972
2	0.029	0.986

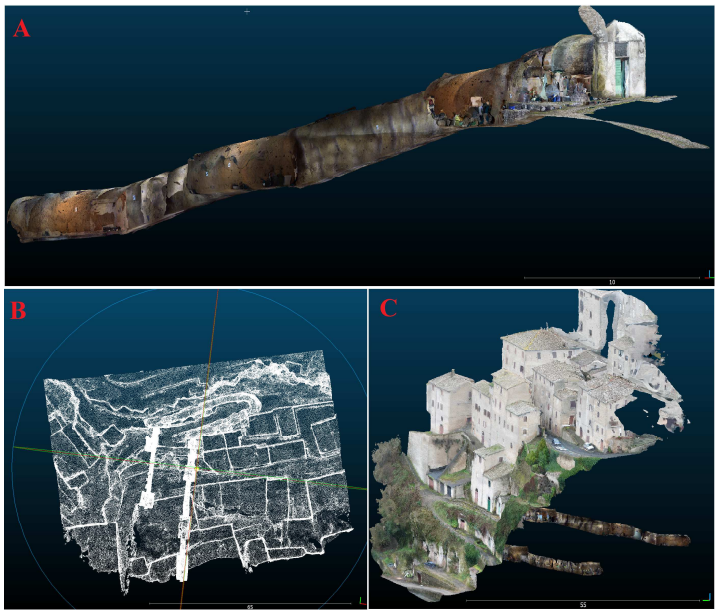

Figure 5. Lidar survey of cavity 2 (**A**), the final alignment of the 3D cavity models with a detail of the depicted UAV survey to visually appreciate the degree of accuracy (**B**), 3D model merged in perspective view (**C**).

Figure 6. Textured 3D model of the north cliff of Grotte di Castro (**A**), photo from UAV, climbed following the photogrammetric process (**B**), photo detail with cavity not accessible on foot (**C**).

The plans of the cavities obtained from the 3D models were compared with those obtained from traditional surveying methods (in this case, the differences between the perimeters and areas) (Figure 7). The results of the comparisons are shown in Table 5.

Table 5. Surfaces and perimeters of cavities.

Cavity	Surface m^2 (iPhone)	Perimeter m (iPhone)	Surface m^2 (Traditional)	Perimeter m (Traditional)
1	63.7	69.44	61.88	68.32
2	133.29	111.52	129.81	110.67

The survey was carried out using traditional methods as the reference survey. The survey carried out with lidar of cavity No. 1 deviates from the reference by 1.12 m for perimeters and 1.82 m^2 for surfaces. The reliefs of cavity n2 deviate from the reference by 0.85 m for perimeters and 3.48 m^2 for surfaces. Still referring to the traditional survey, it is possible to estimate differences between the two methods at around 3% for surfaces and 1.5% for perimeters.

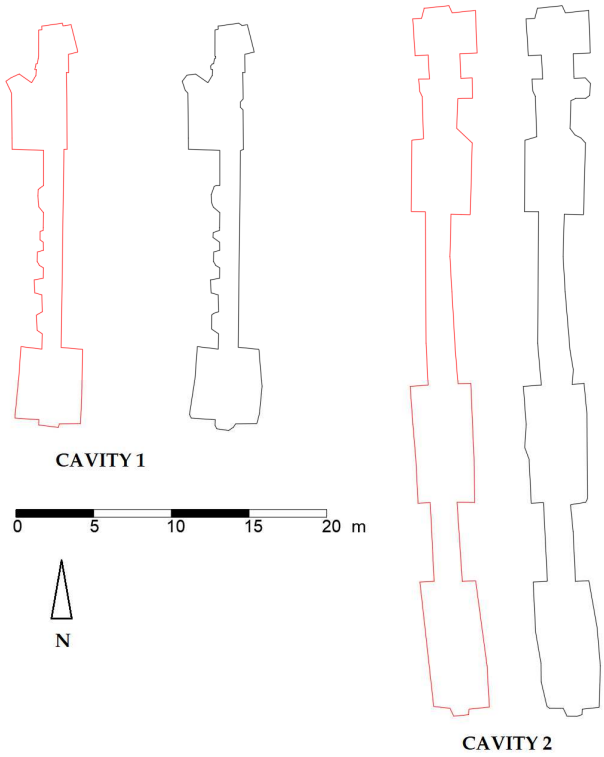

Figure 7. Floor plans of the two cavities: in red the plan obtained using traditional methods. and in black that obtained from lidar surveys.

From the point cloud, the DEM was created, which was used as the basis for the realisation of the orthomosaic. To have a better and more usable representation of the results, the entrances located on the model were exported in .shp format, together with the orthomosaic. These products were loaded into a GIS project realised with QGIS software with the planimetries and exported in .shp format. The projection on the 1:5000 Regional Technical Map of the orthomosaic, planimetries and entrances completed the optimisation of this process, proposing, in fact, a first census of the entrances to the caves on the northern slope of the cliff of Grotte di Castro (Figure 8).

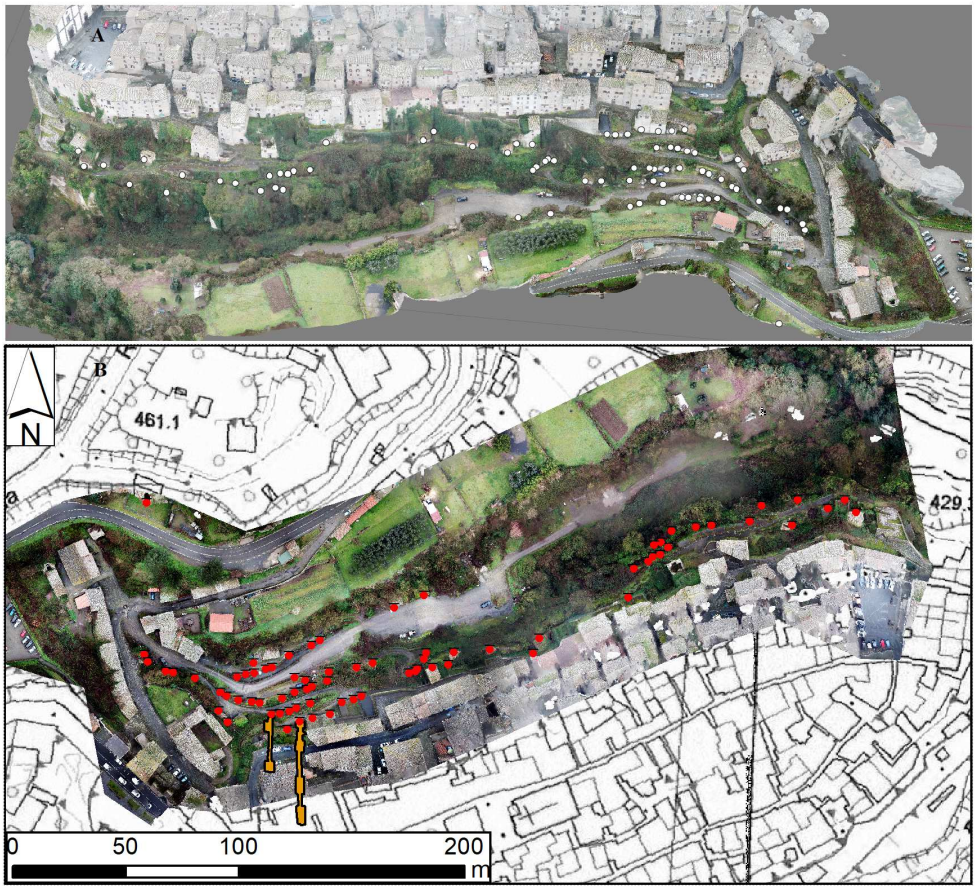

Figure 8. Process of identifying inputs to the model and (**A**) and transferring the data to the GIS environment ((**B**) the entrances in red and the floor plans in yellow).

4.3. Geomechanical Survey and Empirical Evaluation of Stability

The geomechanical survey provided the following parameters for calculating Q, which coincided with the parameter Q' for applying the graphical stability method due to the absence of water and the factor $SFR = 1$. The same classification was obtained in both cavities, indicating the rock mass's local homogeneity (Table 6). Rock Mechanics Geostru software was used to facilitate the calculation operations.

Table 6. Classification of the rock mass.

Cavity	Q'	Classification Class
1	7.5	V (mediocre)
2	7.5	V (mediocre)

Using the Geostone rock sclerometer and ISMR standards, a uniaxial compressive strength of around 10 MPa was estimated. The joints shown in Tables 7 and 8 were surveyed using the compass equipped with a clinometer. The joints have been reported on the stereograms shown in Figure 9.

Table 7. Cavity joints number 1.

Number	Deep Direction (°)	Inclination (°)
1	345	40
2	340	60
3	20	70
4	170	75
5	330	80
6	175	80
7	185	75

Table 8. Cavity joints number 2.

Number	Deep Direction (°)	Inclination (°)
1	340	65
2	170	85
3	355	70
4	95	80
5	355	80
7	185	75
8	170	65
9	170	70

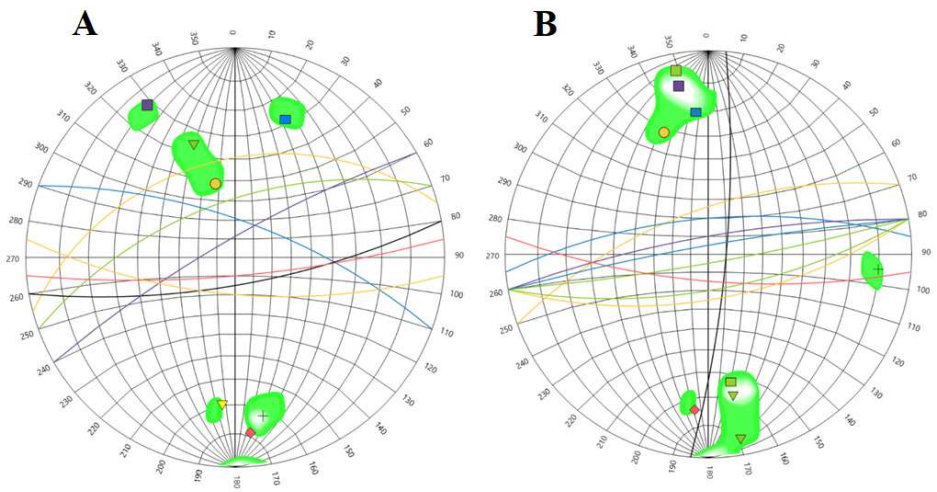

Figure 9. Stereograms of fractures in cavity 1 (**A**) and cavity 2 (**B**).

Using the overall 3D model and sections of the 3D cavity models, geometric parameters, such as hydraulic radius and vault thicknesses, were measured, which are useful for applying empirical stability methods. The operations were repeated for each hall and corridor of the two cavities. The results are shown in Tables 9–12. Figure 10 shows the stability graph with the results.

Table 9. Results of the Critical Scaled Crow Span method cavity 1.

S	T	L	cosθ	CS	Sc
2.3000	5.6500	3.7400	0.9850	1.3123	7.9271
3.5300	12.3600	4.3600	0.9850	1.2864	7.9271
1.2800	23.8100	12.8000	0.9850	0.4311	7.9271
4.3400	24.6300	5.1000	0.9850	1.1078	7.9271

Table 10. Results of the Critical Scaled Crow Span method cavity 2.

S	T	L	cosθ	CS	Sc
4.0100	6.8500	8.5200	0.9850	1.8132	7.9271
3.8400	15.0400	4.8200	0.9850	1.0909	7.9271
1.9000	17.8600	11.2300	0.9850	0.5745	7.9271
4.0200	22.7800	7.5500	0.9850	0.9826	7.9271
1.8000	25.3200	5.0600	0.9850	0.4353	7.9271
3.8700	25.8400	8.5000	0.9850	0.9043	7.9271

Table 11. Results of the Stability Graphical method cavity 1.

Q′	A	B	C (Falls)	C (Sliding)	N (Falls)	N (Sliding)	S
7.5	0.1	0.7	2.1	2.1	1.1025	1.1025	0.65
7.5	0.1	0.7	2.1	2.1	1.1025	1.1025	0.87
7.5	0.1	0.7	1.5	2.1	0.7875	1.1025	0.36
7.5	0.1	0.7	2.1	2.1	1.1025	1.1025	0.78

Table 12. Results of the Stability Graphical method cavity 2.

Q′	A	B	C (Falls)	C (Sliding)	N (Falls)	N (Sliding)	S
7.5	0.1	0.65	1.5	2.1	0.73125	1.02375	1.04
7.5	0.1	0.65	1.5	2.1	0.73125	1.02375	0.88
7.5	0.1	0.65	2.1	2.1	1.02375	1.02375	0.51
7.5	0.1	0.65	1.5	2.1	0.73125	1.02375	0.82
7.5	0.1	0.65	2.1	2.1	1.02375	1.02375	0.49
7.5	0.1	0.65	1.5	2.1	0.73125	1.02375	0.75

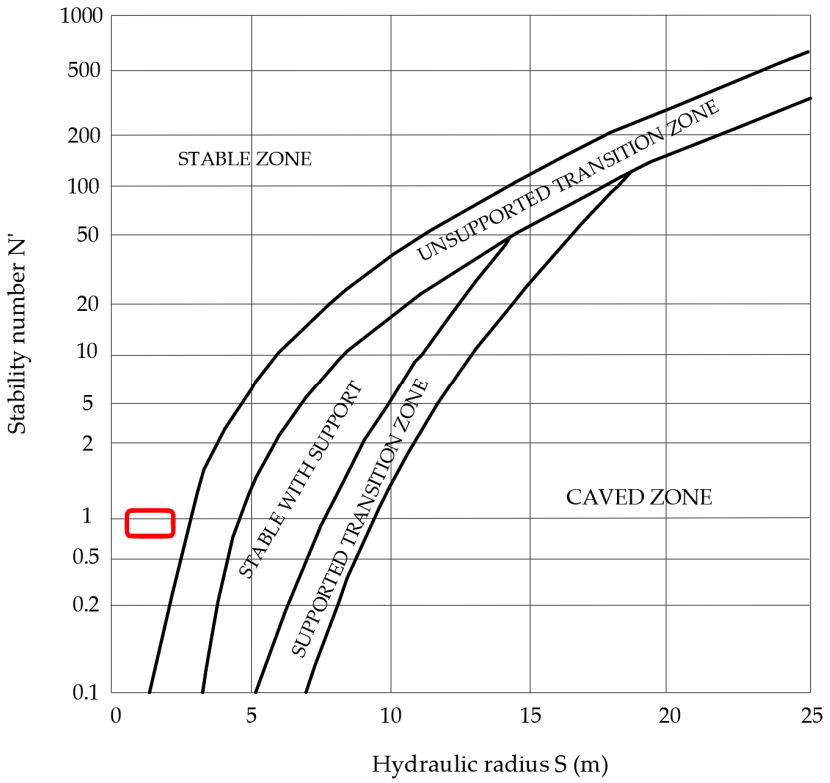

Figure 10. Stability graph projection of all results. All the halls and tunnels of the analysed cavities fall in the red rectangle.

According to the Harp and Noble method, the AF parameter was calculated based on the average joint opening, estimating a value of 2.5 to assess the susceptibility to collapse in the event of an earthquake. This yields a Q'' value, attributable to both cavities, of 10.1, so the propensity to collapse in the event of an earthquake (M > 5) is low, if only slightly.

5. Discussion

Using UAVs made it possible to obtain photogrammetric surveys of a portion of the cliff of Grotte di Castro. The survey obtained with the drone's onboard GPS is characterised by a considerable error (1.7 m), which cannot be used for typographical purposes. Moreover, the elevation associated with it is not, in fact, even traceable to an ellipsoid elevation. This represents a definite limitation that limits this type of survey to initial expeditious censuses to identify the entrances of cavities in a given urban context for which centimetric precision is not required. The data thus obtained can be entered into a GIS environment and digitised. In addition, thanks to the comparison with more detailed maps (e.g., topographic maps at a scale of 1:5000), it is also possible to obtain relatively reliable information on the orthometric height of the entrances to the cavities surveyed in this way. Another advantage of this survey method is the reduction in time. Using the 3D model, 76 entrances along the study area were surveyed in 64 min, taking into account the time required for surveying and obtaining the 3D model. In particular, the search in the model for entrances must be conducted with great care, looking for doors and dark colours, as well as subcircular shapes that could be identified as cavity entrances. One issue that should not be underestimated is vegetation. This problem, closely related to the use of photogrammetry, was considered during the planning phase and partially solved by acquiring frontal and close-up photos. This made it possible to reconstruct points beyond the vegetation, facilitating the identification of cavities not otherwise visible with only nadiral photos (Figure 11). Points that can be classified as vegetation are characterised by low confidence and can be eliminated when editing the point cloud, further facilitating the identification of an entrance or even just a portion. The walking cavity survey took 145 min to survey 58 entrances, as not all were directly accessible due to vegetation and the collapse of the connecting road (Table 3).

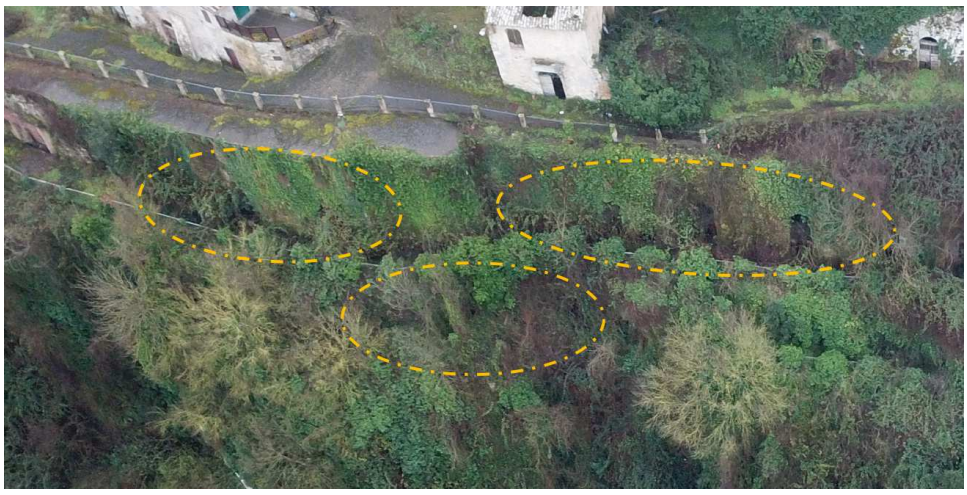

Figure 11. Example of using frontal photos to limit the effects of vegetation. In the orange ovals, some examples of localised entries using frontal photos (inclination of the gimbal 0°–25°).

The problem of accuracy, as already seen in several cases involving natural sinkholes [15] and other issues [21], can be solved by using GNSS stations or drones equipped with GPS PPK-NRTK [14], which significantly reduce errors, but require more time for execution, processing and the use of more expensive instruments. The survey obtained using ground points surveyed with a GNSS station made it possible to identify the same number of cavities whose coordinates, in addition to being associated with greater precision (error

of around 4 cm), are characterised by an exact orthometric height. This type of survey is extremely useful when it is necessary to increase accuracy and analyse interactions between cavities and surfaces. This article also evaluated the performance of a low-cost instrument such as the lidar mounted on the iPhone 15 Pro Max applied to a cavity census. In the recent past, the possible applications of this instrument have been evaluated by comparing it with other methods [18,55,56], finding wide application margins and low errors. The small size of the iPhone 15 Pro Max is well suited to tight spaces and the difficulties of surveying cramped and poorly lit cavities. A comparison of the cavity surveys performed with the iPhone with those performed with traditional methods shows a slight difference, estimated at around 3% for surfaces and 1.5% for perimeters. These differences can be attributed to the impossibility of considering small roughness elements due to the way the cavities are excavated, which characterises the use of traditional methods. However, this type of survey lacks a reliable reference system and orientation in space due to the poor accuracy of the iPhone's GPS. For this reason, the alignment of 3D cavity models to the model obtained from UAV photogrammetry supported by points measured with a GNSS station was evaluated. The alignment method considered in this article evaluates the Cloud Compare software capabilities and the Alings Two Clouds tool, which can also be used with 3D models. The good result obtained (average RMS of the alignments 3.5 cm and scaling factor close to 1) thanks to special ground markers common to both surveys (Figures 4B,C and 12A) made it possible to solve the reference system problem. The models aligned in this way can be used to evaluate possible interconnections between the orientation of the cavity in space and the surface elements that may lie on the vertical of the cavity. The fundamental limitation of the use, found in the execution of surveys, of this lidar instrumentation is the range. It has been found that surveys carried out at distances greater than 5 m do not return reliable profiles with the detail required for alignment operations and cannot be used for geotechnical assessments. The consultation of these models was extremely useful to apply some empirical and simplified methods to assess the stability of these cavities. In addition to providing the necessary geometric information (Figure 12B), it has allowed us to conduct evaluations and fracture modelling of the rock mass hosting the cavities, especially using Cloud Compare's Compass tool (Figures 6A and 12C). The geotechnical parameters determined using known methods [25–27,51], combined with the geometric information, revealed a picture of substantial stability for all the halls and tunnels examined. Rather than the specifics of the rock mass (classed as mediocre and with low uniaxial compression strength values), this stability can be attributed to the shape of the cavities. By examining the hydraulic radii, it can be seen that these are around values between 0.65 and 1.04, which, according to the methods taken into consideration, already provide good stability characteristics. This further emphasises the importance of cavity geometric factors and modelling methods. Considering, however, an event with a magnitude greater than 5, this context evolves towards a situation of less pronounced stability, reaching borderline conditions between a low and medium susceptibility to collapse for seismic events of medium energy.

Figure 12. Examples of good alignment of the lidar model to the photogrammetric point cloud (**A**), use of the aligned and georeferenced 3D model to determine the geometric parameters of the cavity (**B**), identification in the sections of the 3D model of the rock mass joints for in-depth geostructural, geotechnical and stability checks, using the Compass plugin of Cloud Compare (**C**).

6. Conclusions

Photogrammetry and low-cost iPhone lidar techniques can be positively evaluated for approaching cavity surveys to prevent sinkhole risk. From these surveys, it has been possible to obtain various information, such as the positions of the entrances, geometric parameters, evaluations of the geomechanical arrangements of the rock masses and evaluations of the possible interconnections of these cavities with the surface. The varying degrees of accuracy depending on the scaling method of the models is closely related to the degree of precision with which the census is to be carried out. The low costs of the instruments used make this approach easily replicable, especially in rocky settlements such as Grotte di Castro. Other settlements with very different characteristics to those of Grotte di Castro are currently being studied. This methodology is potentially applicable to various types of settlements. By repeating and adapting this methodology in different urban and geographical contexts, it would be possible to hypothesise the drafting of a general low-cost method adaptable to other case studies. By limiting resources, it is, in fact, possible to have reliable models that make it possible to know with good precision the position of the cavities in space and the possible interactions with the surface. By applying empirical stability assessment methods that require basic elements, it is possible to identify areas with a high predisposition to anthropogenic sinkhole formation. In these identified areas, more resources can be concentrated on more thorough risk assessments, especially from a seismic perspective, and on the planning of monitoring networks and safety measures.

Author Contributions: Conceptualization, F.G. and S.M.; methodology, F.G.; software, F.G.; validation, F.G. and S.M.; formal analysis, F.G.; investigation, F.G.; resources, F.G. and S.M.; data curation, F.G. and S.M.; writing—original draft preparation, F.G. and S.M.; writing—review and editing, F.G. and S.M.; visualization, F.G.; supervision, F.G. and S.M.; project administration, S.M.; funding acquisition, S.M. All authors have read and agreed to the published version of the manuscript.

Funding: This research was partially funded by PNRR—European Union—NextGenerationEU—Mission 4 "Education and Research"—Component 2 "From Research to Business"—Investment 3.1 "Fund for the realisation of an integrated system of research and innovation infrastructures". CUP: I53C22000800006.

Data Availability Statement: The datasets presented in this article are not readily available because the data are part of an ongoing study. Requests to access the datasets should be directed to francesco.gentili@unitus.it.

Acknowledgments: We would like to thank the owners of the cavities and the employees of the municipality of Grotte di Castro for their support.

Conflicts of Interest: The authors declare no conflicts of interest.

References

1. Fairbridge. *The Encyclopedia of Geomorphology*; Ed. Reinhold: New York, NY, USA, 1968; 1295p.
2. Nisio, S. The Sinkholes: Teminological Problmes, Genetic Mechanism, Classification. *Mem. Descr. Carta Geol. It.* **2008**, *85*, 17–32.
3. Available online: https://www.isprambiente.gov.it/it/attivita/suolo-e-territorio/sinkholes-e-cavita-sotterranee/classificazione-dei-sinkholes (accessed on 26 March 2024).
4. Ciotoli, G.; Di Loreto, E.; Finoia, M.G.; Liperi, L.; Meloni, F.; Nisio, S.; Sericola, A. Sinkhole susceptibility, Lazio Region, central Italy. *J. Maps* **2016**, *12*, 287–294. [CrossRef]
5. Vennari, C.; Parise, M. A Chronological Database about Natural and Anthropogenic Sinkholes in Italy. *Geosciences* **2022**, *12*, 200. [CrossRef]
6. Delle Rose, M.; Federico, A.; Parise, M. Sinkhole genesis and evolution in Apulia, and their interrelations with the anthropogenic environment. *Nat. Hazards Earth Syst. Sci.* **2004**, *4*, 747–775. [CrossRef]
7. Parise, M.; De Pascalis, A.; De Pascalis, F.; Donno, G.; Inguscio, S. Cavita sotterranee a fini estrattivi, e loro connessione con fenomeni di sprofondamento e subsidenza in agro di Cutrofiano (Lecce). In Proceedings of the Spelaion 2006, Borgo Celano, Italy, 8–10 December 2008; pp. 55–69.
8. Bonamini, M.; Di Maggio, C.; Lollino, P.; Madonia, G.; Parise, M.; Vattano, M. Sprofondamenti di origine antropica nell'area di Marsala (Sicilia occidentale) analizzati mediante rilievi in sito e analisi numerica dei processi di instabilità nelle cave sotterranee. *Mem. Descr. Della Carta Geol. It.* **2013**, *93*, 105–120.
9. Tufano, R.; Guerriero, L.; Annibali Corona, M.; Bausilio, G.; Di Martire, D.; Nisio, S.; Calcaterra, D. Anthropogenic sinkholes of the city of Naples, Italy: An update. *Nat. Hazards* **2022**, *112*, 2577–2608. [CrossRef]
10. Nisio, S.; Caramanna, G.; Ciotoli, G. Sinkholes in Italy: First results on the inventory and analysis. *Geol. Soc. Lond. Spec. Publ.* **2007**, *279*, 23–45. [CrossRef]
11. Madonna, S.; Nisio, S.; Finocchiaro, G.; Gentili, F. Le cavità antropiche presenti nel sottosuolo di Bolsena. *Mem. Descr. Carta Geol. d'It.* **2020**, *107*, 383–396.
12. Madonna, S.; Nisio, S.; Vessella, F. Primo contributo al censimento delle cavità sotterranee di Viterbo. *Mem. Descr. Carta Geol. d'It.* **2021**, *108*, 339–352.
13. Oliveira, S.; Moura, D.; Boski, T.; Horta, J. Coastal paleokarst landforms: A morphometric approach via UAV for coastal management (Algarve, Portugal case study). *Ocean Coast. Manag.* **2019**, *167*, 245–261. [CrossRef]
14. Pingel, T.J.; Saavedra, A.; Cobo, L. Deriving Land and Water Surface Elevations in the Northeastern Yucatán Peninsula Using PPK GPS and UAV-Based Structure from Motion. *Pap. Appl. Geogr.* **2021**, *7*, 294–315. [CrossRef]
15. Puzzilli, L.; Ruscito, V.; Madonna, S.; Gentili, F.; Ruggiero, L.; Ciotoli, G.; Nisio, S. Natural sinkhole monitoring and characterization: The case of Latera sinkhole (Central Italy). *Geosciences* **2024**, *14*, 18. [CrossRef]
16. Monsalve, A.; Yager, E.M.; Tonina, D. Evaluating Apple iPhone LiDAR measurements of topography and roughness elements in coarse bedded streams. *J. Ecohydraulics* **2023**. *early access*. [CrossRef]
17. King, F.; Kelly, R.; Fletcher, C.G. New opportunities for low-cost LiDAR-derived snow depth estimates from a consumer drone-mounted smartphone. *Cold Reg. Sci. Technol.* **2023**, *207*, 103757. [CrossRef]
18. Díaz-Vilariño, L.; Tran, H.; Frías, E.; Balado, J.; Khoshelham, K. 3D Mapping of Indoor And Outdoor Environments Using Apple Smart Devices. *ISPRS-Int. Arch. Photogramm. Remote Sens. Spat. Inf. Sci.* **2021**, *43-B4*, 303–308. [CrossRef]
19. Teo, T.A.; Yang, C.C. Evaluating the accuracy and quality of an iPad Pro's built-in lidar for 3D indoor mapping. *Dev. Build Environ.* **2023**, *14*, 100169. [CrossRef]
20. Rutkowski, W.; Lipecki, T. Use of the iPhone 13 Pro LiDAR Scanner for Inspection and Measurement in the Mineshaft Sinking Process. *Remote Sens.* **2023**, *15*, 5089. [CrossRef]

21. Silva, O.L.; Bezerra, F.H.R.; Maia, R.P.; Cazarin, C.L. Karst landforms revealed at various scales using LiDAR and UAV in semi-arid Brazil: Consideration on karstification processes and methodological constraints. *Geomorphology* **2017**, *295*, 611–630. [CrossRef]
22. I.S.R.M. (International Society for Rock Mechanics). Suggested methods for the quantitative description of discontinuities in rock masses. *Int. J. Rock Mech. Min. Sci. Geomech. Abstr.* **1978**, *15*, 319–368.
23. I.S.R.M. (International Society for Rock Mechanics). Basic geotechnical description of rock masses. *Int. J. Rock Mech. Min. Sci. Geom. Abstr.* **1981**, *18*, 85–110.
24. I.S.R.M. (International Society for Rock Mechanics). *Rock Characterization, Testing and Monitoring*; Brown, E.T., Ed.; Pergamon Press: Oxford, UK, 1981; p. 211.
25. Harp, E.L.; Noble, M.A. An Engineering Rock Classification to Evaluate Seismic Rock-Fall Susceptibility and its Application to the Wasatch Front. *Environ. Eng. Geosci.* **1993**, *30*, 293–319. [CrossRef]
26. Carter, T.G. A new approach to surfacecrown pillar design. In Proceedings of the 16th Canadian Rock Mechanics Symposium, Sudbury, ON, Canada; 1992; pp. 75–83.
27. Potvin, Y.; Milne, D. Empirical cable bolt support design. In *Rock Support in Mining and Underground Construction. In Proceedings of the 16th Canadian Rock Mechanics Symposium. Sudbury, ON, Canada, 1992*; Kaiser, P.K., McCreath, D.R., Eds.; Balkema: Rotterdam, The Netherlands, 1992.
28. Zhao, X.; Li, H.; Zhang, S.; Yang, X. Stability Analyses and Cable Bolt Support Design for A Deep Large-Span Stope at the Hongtoushan Mine, China. *Sustainability* **2019**, *11*, 6134. [CrossRef]
29. Sapia, V.; Materni, V.; Florindo, F.; Marchetti, M.; Gasparini, A.; Voltattorni, N.; Civico, R.; Giannattasio, F.; Miconi, L.; Marabottini, M.F.; et al. Imaging multiparametrico di tombe a camera etrusche: Caso di studio Grotte Di Castro (Italia). *Appl. Sci.* **2021**, *11*, 7875. [CrossRef]
30. Ciotoli, G.; Finoia, M.G.; Liperi, L.; Meloni, F.; Nisio, S.; Tonelli, V.; Zizzari, P. Sinkhole susceptibility map of the Lazio Region, central Italy. *J. Maps* **2015**, *12*, 287–294. [CrossRef]
31. Washington, H.S. *The Roman Comagmatic Rgion*; Carnegie Institute Washington: Washington, DC, USA, 1906; Volume 36, pp. 1–220.
32. Locardi, E.; Lombardi, G.; Funiciello, R.; Parotto, M. The main volcanic groups of the Latium (Italy): Relations between structural evolution and petrogenesis. *Geol. Romana* **1976**, *16*, 279–300.
33. Sparks, R.S.J. Stratigraphie et géologie des ignimbrites du volcan Vulsini, Italie centrale. *Geol. Rundsch.* **1975**, *64*, 497–523. [CrossRef]
34. Peccerillo, A. *Cenozoic Volcanism in the Tyrrhenian Sea Region*; Springer: Berlin/Heidelberg, Germany, 2017. [CrossRef]
35. Nappi, G.; Renzulli, A.; Santi, P. An evolutionary model for the Paleo-Bolsena and Bolsena volcanic complexes: A structural and petrographic study. *Per Miner.* **1987**, *56*, 241–267.
36. Nappi, G.; Renzulli, A.; Santi, P. Evidence of incremental growth in the Vulsinian calderas (central Italy), in Verma-Surendra, P., ed., Calderas: Genesis, Structure and Unrest. *J. Volcanol. Geotherm. Res.* **1991**, *47*, 13–31. [CrossRef]
37. Vezzoli, L.; Conticelli, S.; Innocenti, F.; Landi, P.; Manetti, P.; Palladino, D.M.; Trigila, R. Stratigraphy of the Latera volcanic complex: Proposals for a new nomenclature. *Period. Mineral.* **1987**, *56*, 89–110.
38. Metzelin, S.; Vezzoli, L. Santa Contributi alla geologia del Vulcano di Latera (Monti Vulsini, Toscana meridionale, Lazio settentrionale). *Mem. Soc. Geol. It.* **1983**, *25*, 247–273.
39. Turbeville, B.N. Tephra fountaining, rheomorphism, and spatter flow during emplacement of the Pitigliano Tuffs, Latera caldera, Italy. *J. Volcanol. Geotherm. Res.* **1992**, *53*, 309–327. [CrossRef]
40. Palladino, D.M.; Simei, S.; Sottili, G.; Trigila, R. Integrated approach for the reconstruction of stratigraphy and geology of Quaternary volcanic terrains: An application to the Vulsini Volcanoes (central Italy). In *Stratigraphy and Geology in Volcanic Areas*; Groppelli, G., Viereck-goette, L., Eds.; Geological Society of America: Boulder, CO, USA, 2010; Volume 464, pp. 66–84. [CrossRef]
41. Valerio, A.; Danilo, P.; Raffaello, C.; Russo, P.; Simei, S. Caldera structure, amount of collapse, and erupted volumes: The case of Bolsena caldera, Italy. *Geol. Soc. Am. Bull.* **2012**, *124*, 1562–1576. [CrossRef]
42. Bizzarri, R.; Ambrosetti, P.; Argenti, P.; Gatta, G.; Baldanza, A. L'affioramento del Caio (Lago di Corbara, Orvieto, Italia Centrale) nell'ambito dell'evoluzione paleogeografica Plio-Pelistocenica della Valle del Tevere: Evidenze sedimentologiche e stratigrafiche. *Il Quat.* **2003**, *16*, 241–255.
43. Bizzarri, R.; Baldanza, A.; Petrelli, M.; Famiani, F.; Peccerillo, A. Early Pleistocene distal pyroclastic-fallout material in continental and marine deposits of Western Umbria (Italy): Chemical composition, provenance and correlation potential. *Il Quat.* **2010**, *23*, 245–250.
44. Available online: https://idrogeo.isprambiente.it/app/pir?@=41.55172525858242,12.573501484000001,2 (accessed on 12 April 2024).
45. Available online: https://www.isprambiente.gov.it/it/attivita/suolo-e-territorio/cartografia/carte-geologiche-e-geotematiche/carta-geologica-alla-scala-1-a-100000 (accessed on 10 April 2024).
46. Palladino, D.M.; Pettini, M. Source- vs. topographic-forcing in pyroclastic currents: The case of the Orvieto-Bagnoregio Ignimbrite, Vulsini, central Italy. *Period. Mineral.* **2020**, *89*, 217–229.
47. Cloud Compare (version 2.1) [GPL Software]. 2024. Available online: http://www.cloudcompare.org/ (accessed on 15 February 2024).

48. Barton, N. Rock mass classification, tunnel reinforcement selection using the Q-system. In *Rock Classification Systems for Engineering Purposes*; ASTM International: West Conshohocken, PA, USA, 1987.
49. Barton, N.; Lien, R.; Lunde, J. Engineering classification of rock masses for the design of tunnel support. *Rock Mech.* **1974**, *6*, 188–236. [CrossRef]
50. Brown, E.T.; Bray, J.W.; Ladanyi, B.; Hoek, E. Characteristic line calculations for rock tunnels. *J. Geotech. Engng Div. ASCE* **1983**, *109*, 15–39. [CrossRef]
51. Carter, T.G. *Guidelines for use of the Scaled Span Method for Surface Crown Pillar Stability Assessment*; Ontario Ministry of Northern Development and Mines: Toronto, ON, Canada, 2014; pp. 1–34.
52. Hoek, E.; Brown, E.T. Empirical strength criterion for rock masses. *J. Geotech. Eng. Div.* **1980**, *106*, 1013–1035. [CrossRef]
53. Hoek, E.; Brown, E.T. *Underground Excavations in Rock*; Institute of Mining and Metallurgy: London, UK, 1980.
54. Hoek, E.; Brown, E.T. Practical estimates of rock mass strength. *Int. J. Rock Mech. Min. Sci.* **1997**, *34*, 1165–1186. [CrossRef]
55. Luetzenburg, G.; Kroon, A.; Bjørk, A.A. Evaluation of the Apple iPhone 12 Pro LiDAR for an Application in Geosciences. *Sci. Rep.* **2021**, *11*, 22221. [CrossRef]
56. Tavani, A.; Billi, A.; Corradetti, A.; Mercuri, M.; Bosman, A.; Cuffaro, M.; Seers, T.; Carminati, E. Smartphone assisted fieldwork: Towards the digital transition of geoscience fieldwork using LiDAR-equipped iPhones. *Earth-Sci. Rev.* **2022**, *227*, 103969. [CrossRef]